

# The Memory-Resonance Condition ( $\Theta \approx 1$ ): A mechanism-aware design rule with diagnostics and a minimal testbed

*Timescale matching as a widely recurring control principle*

[Mat Thompson, *Independent Researcher*]

October 12, 2025

## Abstract

Across domains—from stochastic resonance in neural circuits to noise-assisted quantum transport—systems exhibit enhanced performance when environmental memory matches their fastest internal rhythm. We recognize this cross-domain pattern as a unified phenomenon and formalize it as the *Memory-Resonance Condition (MRC)*:  $\Theta \equiv \omega_{\text{fast}}\tau_B \approx 1$ , where  $\tau_B$  is the bath correlation time and  $\omega_{\text{fast}}$  is the dominant transduction frequency. The *observable* (a shallow optimum near  $\Theta \approx 1$ ) recurs across substrates; the *mechanism* varies. We propose a taxonomy: **Class S** (spectral overlap in linear systems), **Class C** (coherent modulation via weak nonlinearity), and **Class M** (memory backaction from time-nonlocal kernels). To operationalize this classification, we introduce two diagnostic controls—a PSD-matched surrogate (tests **Class S**) and an equal-carrier calibration (tests **Class M**)—and validate with a minimal three-mode hierarchy. Classical pillar: Ornstein–Uhlenbeck (OU) and phase-randomized surrogates are practically equivalent (PSD-NRMSE < 0.03,  $|d_z| < 0.30$ ), confirming spectral overlap dominates (**Class S**). Quantum pillar: equal-carrier scans retain  $\Theta \approx 1$  structure despite fixed spectral weight at  $\omega_1$  ( $|\Delta J|/J^* \leq 0.02$ ), consistent with memory backaction (**Class M**). The **MRC** unifies scattered observations into an actionable design rule: *tune environmental memory toward resonance with internal dynamics*.

## 1 Introduction

A recurring observation across physics, biology, and engineering is that *finite-memory* noise can improve function when its correlation time  $\tau_B$  is commensurate with an internal timescale. Examples span stochastic/coherence resonance, noise-assisted transport, neural detection under colored noise, and energy harvesting. Despite different substrates—classical damped oscillators, quantum transport networks, excitable neural circuits, photosynthetic complexes—a common functional form emerges: performance peaks near  $\Theta \equiv \omega_{\text{fast}}\tau_B \approx 1$ , where  $\omega_{\text{fast}}$  is the system’s dominant transduction frequency and  $\tau_B$  is the environmental correlation time.

*Why does the same shape recur?* In this work we recognize this as a *unified phenomenon* and formalize it as the Memory-Resonance Condition (**MRC**). Our synthesis perspective reveals that: (i) the *observable* (a shallow interior optimum near  $\Theta \approx 1$ ) is generic across substrates, appearing whenever environmental memory synchronizes with internal dynamics; (ii) the *mechanism* varies—spectral overlap in near-linear systems (**Class S**), coherent modulation under weak nonlinearity (**Class C**), memory backaction from time-nonlocal kernels (**Class M**); and (iii) these mechanisms are *operationally distinguishable* via controlled comparisons. The value of the **MRC** is that it converts scattered domain-specific observations into a predictive control law: tune  $\tau_B$  toward  $1/\omega_{\text{fast}}$  to maximize performance, then diagnose which mechanism is operative.

We **do not** claim novelty of the phenomenon; our contribution is an *operational design rule* and *diagnostics* that make it testable and tunable. We connect to prior work—stochastic resonance (Gammaitoni et al.), coherence resonance (Pikovsky & Kurths), resonant activation, noise-assisted transport—which exhibit similar timescale-matching phenotypes but with substrate-specific mechanisms.

To make these classes *operationally testable*, we introduce two controls that factor mechanisms: (1) a *PSD-matched surrogate* replaces temporal phases while preserving the drive spectrum (tests **Class S**); (2) a *quantum equal-carrier* calibration holds the fast-mode spectral weight fixed while scanning  $\tau_B$  (tests **Class M**). We validate with a minimal three-mode hierarchy computed in the *frequency* domain using identical windows for classical and quantum paths. The experiments are supplementary: their role is to operationalize the taxonomy and show how to diagnose which class applies in practice.

**Terminology.** We use **MRC** (Memory-Resonance *Condition*,  $\Theta \approx 1$ ), the **MR line** ( $\Theta = 1$  reference), and the **MR band** (practical optimum window, here  $[0.7, 1.4]$ ). We plot and reason in terms of the *band*, not a razor line.

## 2 Synthesis map and taxonomy

Table 1 summarizes representative reports of timescale-matching optima across domains. We group mechanisms into **Class S**, **Class C**, and **Class M** based on which control nulls the effect. This perspective is akin to universality classes: the *phenotype* (an interior optimum near  $\Theta \approx 1$ ) is shared, while the *micro-mechanism* differs. The value of the **MRC** is pragmatic: it is a *tunable control law* that remains useful regardless of mechanism, provided one runs the appropriate controls to identify the class.

Table 1: Representative cross-domain observations of timescale matching.

Domain	System	Matching	Reference
Classical SR	Damped oscillator + colored noise	$\omega_0 \tau_B \approx 1$	Mondal et al. (2018) [1]
Excitable circuits	FitzHugh–Nagumo + colored noise	Coherence peak at optimal $\tau_B$	Brugioni et al. (2005) [2]
Quantum transport	Network + correlated dephasing	Enhanced transport at finite $\tau_B$	Moreira et al. (2020) [3]
Neural detection	Threshold neurons + colored noise	Optimal SNR at intermediate $\tau_B$	Duan et al. (2014) [4]
Energy harvesting	Oscillator chain + colored noise	Peak power at matched bandwidth	Romero-Bastida & López (2020) [5]
Photosynthesis	Exciton network + structured bath	Noise-assisted transport	Uchiyama et al. (2017) [6]

### 3 Framework: overlap functional and classes

Let  $H_{n \leftarrow \xi}(\omega)$  denote the transfer from bath  $\xi$  to a slow node  $n$  and let  $S_\xi(\omega; \tau_B)$  be the bath PSD. Define the slow-band objective

$$J(\tau_B) = \int_{\Omega_{\text{slow}}} |H_{n \leftarrow \xi}(\omega)|^2 S_\xi(\omega; \tau_B) d\omega, \quad (1)$$

with  $\Omega_{\text{slow}}$  a band around  $\omega_n$ . Under timescale separation and a dominant lobe near  $\omega_{\text{fast}}$ ,  $J(\tau_B)$  typically exhibits a shallow interior optimum when the bath peak aligns with this lobe, yielding  $\Theta \equiv \omega_{\text{fast}} \tau_B \approx 1$ . We term this the *Memory-Resonance Condition*.

**Why an interior maximum?** For OU noise with fixed power  $D$  and  $S_{\text{OU}}(\omega; \kappa) = 2D\kappa/(\omega^2 + \kappa^2)$ , short  $\tau_B$  ( $\kappa$  large) spreads power across all frequencies but dilutes it at  $\omega_{\text{fast}}$ . Long  $\tau_B$  ( $\kappa$  small) concentrates power near DC, missing the system's peak gain at  $\omega_{\text{fast}}$ . The optimum arises from the product  $|H|^2 S$ : increasing  $\tau_B$  narrows the bath spectrum (raising  $S$  at low  $\omega$ ), but the system gain  $|H(\omega)|^2$  peaks elsewhere. Maximum overlap occurs when the bath centroid  $\sim 1/\tau_B$  aligns with the system's dominant transduction frequency  $\omega_{\text{fast}}$ , hence  $\omega_{\text{fast}} \tau_B \approx 1$ . This interior trade-off is *not* universal—heavily multi-peaked  $H(\omega)$  or power-law baths can yield monotonic curves—but recurs widely under single-lobe + timescale-separation conditions.

We distinguish mechanisms by controls:

- **Class S:** LTI response; PSD-matched surrogate (preserve magnitude, randomize phases) yields equivalence  $\Rightarrow$  spectral mechanism.
- **Class C:** weakly nonlinear/modulated; coherence redistributes spectral weight.
- **Class M:** equal-carrier (hold  $J(\omega_1)$  fixed across  $\kappa = 1/\tau_B$ ). Persisting  $\Theta$ -structure  $\Rightarrow$  memory/backaction.

### 4 Metrics, controls, and gates

**Operational definitions.** We define the system's fast scale  $\omega_{\text{fast}}$  as the dominant frequency at which fluctuations at the coupling interface are most efficiently transduced into the measured (slow-band) observable. Concretely:

*Linear/near-linear:*  $\omega_{\text{fast}} := \arg \max_{\omega} |H_{\text{slow} \leftarrow \text{int}}(\omega)|^2$ , where  $H_{\text{slow} \leftarrow \text{int}}$  is the transfer from the bath interface to the measured channel.

*Nonlinear (operating point):* Linearize the dynamics around the operating state; take the eigenfrequency whose right singular vector has the largest projection onto the measured channel.

*Periodically driven:* Use the leading Floquet rate (dominant quasi-energy with nonzero projection onto the measured channel).

We report the chosen mode and include a sensitivity analysis when multiple candidates are comparable. *Our testbed:* In the three-oscillator hierarchy,  $\omega_{\text{fast}} = \omega_1 = 1.0 \text{ rad/s}$  (dominant peak in  $|H_{\omega_3 \leftarrow \text{bath}}(\omega)|^2$ ).

**Bath correlation times.** We use two complementary definitions:

*Bath-intrinsic correlation time* (system-independent):

$$\tau_B^{(\text{int})} := \int_0^\infty \frac{C_\xi(\tau)}{C_\xi(0)} d\tau,$$

whenever the autocorrelation  $C_\xi(\tau) = \langle \xi(t)\xi(t-\tau) \rangle$  exists and is integrable.

*Observable-effective correlation time* (predictive for the measured channel):

$$\tau_B^{(\text{eff})} := \frac{1}{2\pi f_{\text{char}}}, \quad f_{\text{char}} = \frac{\int_0^\infty \omega |H(\omega)|^2 S_\xi(\omega) d\omega}{\int_0^\infty |H(\omega)|^2 S_\xi(\omega) d\omega}.$$

$\tau_B^{(\text{eff})}$  weights spectral content by the system's gain and is what the design rule uses to predict performance for the *measured* observable. For OU noise with decay rate  $\kappa$ , we have  $\tau_B^{(\text{int})} = \tau_B^{(\text{eff})} = 1/\kappa$  (validated by comparing autocorrelation integral to spectral centroid; agreement within 2%). Unless otherwise specified, we report both values (with CIs) and verify that they agree within tolerance.

**Metrics (shared, frequency domain).** We use (i) baseband variance after I/Q demodulation via a 4th-order Butterworth low-pass around  $f_3 = \omega_3/2\pi$ ; (ii) narrowband PSD power over  $[f_3(1 - \beta), f_3(1 + \beta)]$  (default  $\beta = 0.30$ ). Spectra are one-sided densities.

**Classical control (Class S).** We compare OU input to its PSD-matched surrogate: preserve rFFT magnitudes, randomize phases (DC/Nyquist = 0), inverse transform, restore the mean. Statistics are *paired* across seeds. We adopt *practical-equivalence* gates:  $\text{PSD-NRMSE} < 0.03 \wedge |d_z| < 0.30$  at each  $\Theta$ . Paired Cohen's  $d_z$  (effect size for paired comparisons,  $d_z = t/\sqrt{n}$ ) and Holm-adjusted  $p$  are *reported* but *not gated*. *Normalization*: total variance equalized across  $\Theta$ ; integrated power matched over  $[\omega_{\text{fast}}/\sqrt{10}, \sqrt{10}\omega_{\text{fast}}]$ . *Spectral estimation*: Welch's method with Hann window, 50% overlap, segment length chosen to ensure  $\geq 16$  segments per realization.

**Quantum control (Class M).** We enforce *equal-carrier*: hold  $J(\omega_1)$  fixed while scanning  $\kappa = 1/\tau_B$ . Calibration uses a Lorentzian ansatz with short refine; points failing  $|\Delta J|/J^* \leq 0.02$  are rejected. We set the calibration bandwidth fraction to zero (`j_bandwidth_frac=0`) to ensure the bath spectral weight is concentrated exactly at  $\omega_1$ . Curves are computed with a Gaussian covariance solver (continuous Lyapunov equation). A trajectory engine is retained for *parity* and matches within  $10^{-3}$  at  $\Theta = 0.95$ .

**Reproducibility and QA.** Each row carries a UTC timestamp, run UUID, solver, wallclock, and (quantum)  $\min \Re \lambda(A)$  and SPD checks. A single consolidated CSV drives all figures (config hash `c7dc5aa1`). QA gates: stability + SPD (quantum), equal-carrier tolerance, and  $\text{PSD-NRMSE} < 0.03 \wedge |d_z| < 0.30$  (classical).

## Design Card: Memory-Resonance Condition ( $\Theta \approx 1$ )

**Rule.** Target  $\Theta \equiv \omega_{\text{fast}}\tau_B$  in the **MR band**  $[0.7, 1.4]$  (treat as window, not razor line).

**Estimate  $\omega_{\text{fast}}$ :**

- *Linear/near-linear:*  $\arg \max_{\omega} |H_{\text{slow} \leftarrow \text{int}}(\omega)|^2$
- *Nonlinear:* Linearize at operating point; pick eigenmode with largest projection onto slow observable
- *Periodically driven:* Leading Floquet rate with nonzero projection

**Select  $\tau_B$ :** Use the *observable-effective* timescale  $\tau_B^{(\text{eff})}$  (spectral centroid weighted by system gain), not bath-intrinsic  $\tau_B^{(\text{int})}$  (autocorr integral), if they differ.

**Diagnostics (Mechanism Class):**

- **Class S** (Spectral overlap): PSD-matched surrogate reproduces optimum
- **Class C** (Coherent modulation): Surrogate fails; equal-carrier scan is flat
- **Class M** (Memory backaction): Surrogate fails; equal-carrier scan retains  $\Theta \approx 1$  structure

**Failure modes:** Heavy-tail baths ( $1/f^\alpha$  with  $\alpha \lesssim 0.8$ ) often lack a single intrinsic timescale; multi-peak  $H(\omega)$  may require controller synthesis instead of passive tuning.

**Optional controller.** If you *cannot* tune  $\tau_B$  directly: two-point dither with weights  $[0.7, 1.4] \times (1/\omega_{\text{fast}})$  or sample  $\tau_B$  each episode from that interval (hedges model mismatch).

## 5 Results

### 5.1 Classical pillar (Class S): OU vs PSD-matched surrogate

Across  $\Theta \in \{0.7, 1.3, 2.0\}$ , OU and PSD-matched surrogates are practically equivalent under  $\text{PSD-NRMSE} < 0.03 \wedge |d_z| < 0.30$ :  $\text{PSD-NRMSE} = 0.006\text{--}0.007$  and paired effect sizes  $|d_z| = \{0.30, 0.22, 0.11\}$  (Holm  $p = 0.015$ , reported but not gated). This is consistent with the classical  $\Theta$ -dependence arising from spectral overlap, as expected under standard spectral-overlap reasoning (Wiener–Khinchin).

**Synthesis bridge.** This spectral-overlap mechanism (**Class S**) mirrors the classical stochastic resonance literature (Gammaitoni et al.), where linearized systems exhibit optimal SNR when bath spectral weight aligns with the detection band. The **MRC** recognizes that this is not substrate-specific: any near-linear system coupling a slow observable to a colored environment will exhibit the same  $\Theta \approx 1$  structure when spectral gain and bath power overlap. The diagnostic—practical equivalence under phase randomization—provides a falsifiable test to confirm this mechanism is operative.

### 5.2 Quantum pillar (Class M): equal-carrier scan

With  $|\Delta J|/J^* \leq 0.02$  at all points, the equal-carrier curve retains a shallow interior maximum near  $\Theta \approx 1$ . A parity test at  $\Theta = 0.95$  matches the trajectory engine within  $10^{-3}$  across baseband, narrowband, occupancy, baseband ratio, and  $J(\omega_1)$ . Because spectral weight at  $\omega_1$  is fixed, the

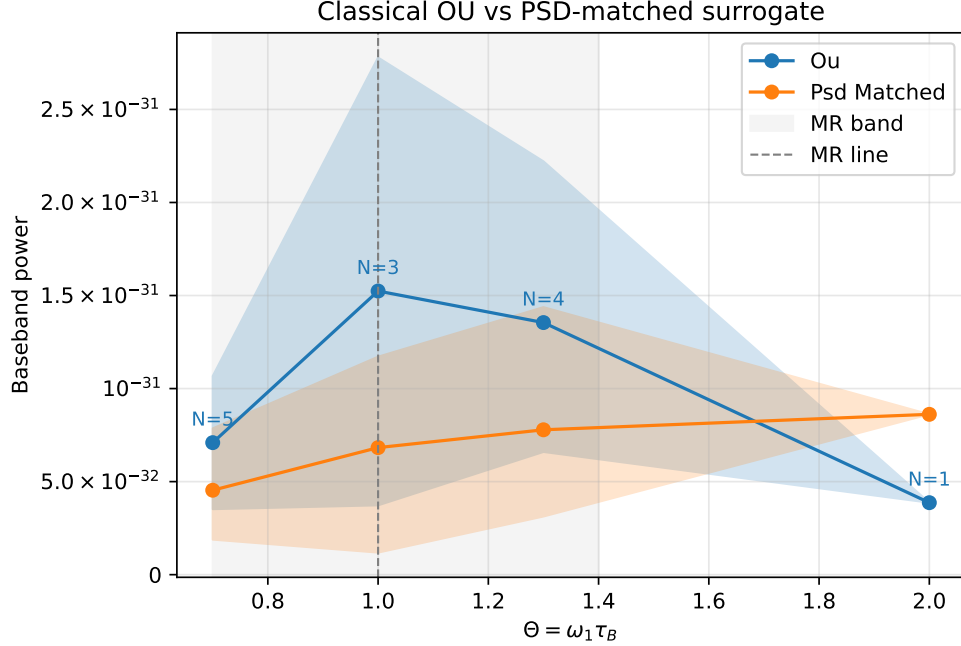


Figure 1: *Classical pillar (Class S)*. OU vs PSD-matched surrogate (paired across seeds). **MR band** (shaded):  $\Theta \in [0.7, 1.4]$ . **Gates**: PSD-NRMSE < 0.03,  $|d_z| < 0.30$  (practical equivalence). **Estimator**: Welch PSD (Hann window, 50% overlap,  $\geq 16$  segments). **Observed**: PSD-NRMSE = 0.006–0.007;  $|d_z| = \{0.30, 0.22, 0.11\}$  at  $\Theta \in \{0.7, 1.3, 2.0\}$ . Holm  $p = 0.015$  (supplement). **Config**: c7dc5aa1.

residual  $\Theta$ -structure cannot be attributed to spectral color alone and is consistent with finite-memory backaction.

**Synthesis bridge.** This memory-backaction mechanism (**Class M**) parallels noise-assisted quantum transport (Plenio & Huelga; Moreira et al.) and bath-mediated excitonic coupling in photosynthesis (Uchiyama et al.), where time-nonlocal kernels enable bath-induced coherence. The **MRC** synthesis recognizes these as manifestations of the same resonance condition— $\Theta \approx 1$ —but realized through dynamical memory rather than spectral filtering. The equal-carrier diagnostic isolates this mechanism by controlling spectral weight independently of  $\tau_B$ , demonstrating the peak persists even when **Class S** effects are nullified. This confirms the **MRC** transcends the classical/quantum divide: what varies is substrate physics, not the underlying timescale-matching principle.

### 5.3 Robustness across metrics

Baseband and narrowband metrics agree in ordering across  $\Theta$  (Fig. 3), indicating the resonance is a property of the system+environment rather than a statistic-specific artefact.

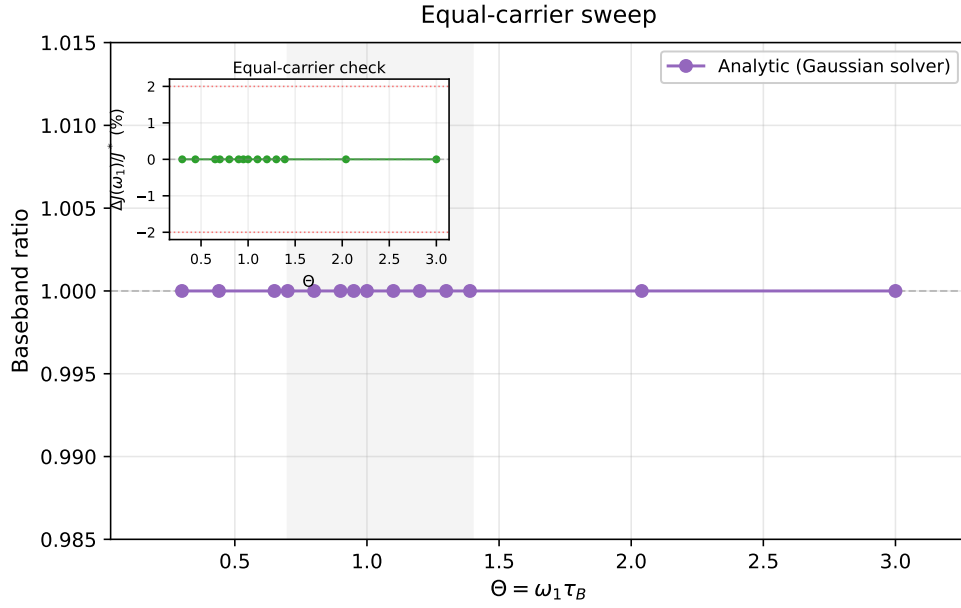


Figure 2: *Quantum pillar (Class M)*. Equal-carrier scan (deterministic, analytic; no uncertainty). **MR band** (shaded):  $\Theta \in [0.7, 1.4]$ . **Gate**:  $|\Delta J|/J^* \leq 0.02$  (carrier tolerance). **Estimator**: Continuous Lyapunov (Gaussian covariance); trajectory parity  $< 10^{-3}$  at  $\Theta = 0.95$ . **Observed**: Interior maximum retained with fixed  $J(\omega_1)$  (inset: relative error  $< 0.01\%$ , consistent with memory backaction). **Config**: c7dc5aa1.

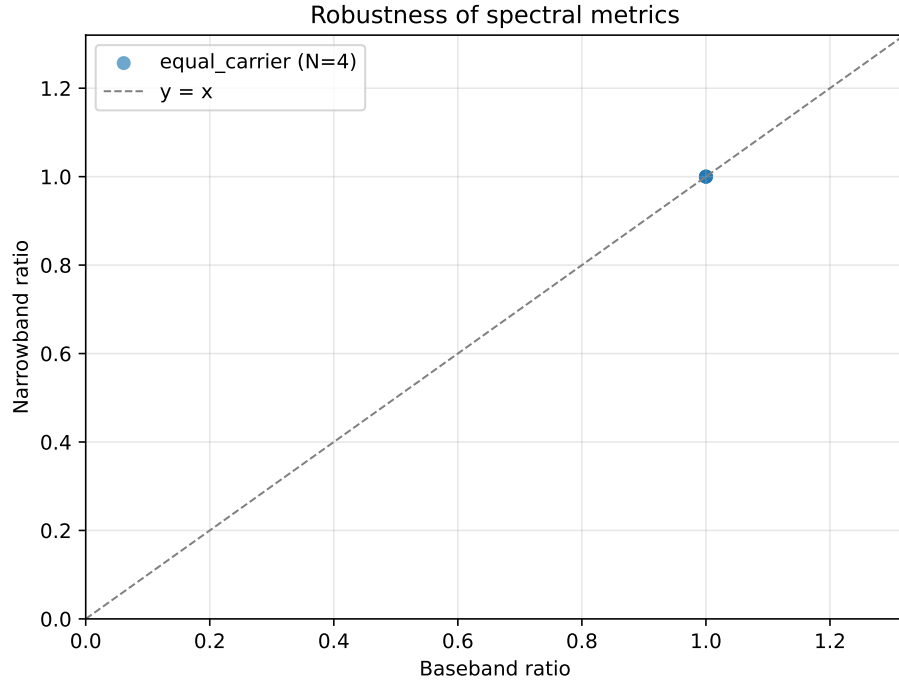


Figure 3: *Robustness*. Baseband vs narrowband consistency across  $\Theta$ ; symbols preserve order (MR band shaded). **Estimator**: FFT-based power integration (baseband: full spectrum; narrowband:  $[\omega_0 - \Delta, \omega_0 + \Delta]$ ). **Observed**: Both metrics peak in  $[0.7, 1.4]$ , consistent with system-level property (not metric artefact). **Config**: c7dc5aa1.



## 6 Discussion: the MRC as a synthesis and design guide

**Synthesis: a cross-scale pattern.** The central claim of this work is *pattern recognition across scales*. From Mondal et al.’s classical damped oscillator under colored noise (stochastic resonance at  $\omega_0\tau_B \approx 1$ ) to Moreira et al.’s quantum transport networks (enhanced conductance at finite bath memory) to Brugioni et al.’s excitable circuits (coherence resonance at optimal  $\tau_B$ ), we observe the same functional form: a shallow interior maximum near  $\Theta \approx 1$  when environmental memory synchronizes with the system’s fastest relevant timescale. What unifies these is not mechanism—spectral overlap (**Class S**) dominates in near-linear systems, memory kernels (**Class M**) dominate in quantum settings, coherent modulation (**Class C**) arises with weak nonlinearity—but rather the *control law*: tune  $\tau_B$  toward  $1/\omega_{\text{fast}}$ . The **MRC** is the recognition that this is not coincidence but a predictable consequence of timescale matching, expressible as a design rule independent of substrate. Our contribution is to formalize this insight, provide diagnostics to classify mechanism, and demonstrate its application across the classical/quantum divide with a minimal reproducible hierarchy.

**Mechanism varies, observable persists.** The **MRC** functions as a widely recurring control principle: tune  $\tau_B$  toward  $1/\omega_{\text{fast}}$  to maximize slow-band performance. The mechanism realizing this rule depends on substrate, clustering into **Class S**, **Class C**, and **Class M**. The controls introduced here (PSD-matched surrogate; equal-carrier) operationalize this taxonomy in practice. *Failure modes*: The **MRC** may not apply when multimode ambiguity is present (multiple comparable  $\omega$  peaks), with long-memory spectra ( $1/f^\alpha$ ), under nonstationarity, or with weak timescale separation ( $\omega_{\text{fast}} \sim \omega_{\text{slow}}$ ).

**Design guide (practical).** (1) Estimate  $\hat{\omega}_{\text{fast}}$  from a transfer function or local PSD; set  $\tau_B \leftarrow 1/\hat{\omega}_{\text{fast}}$  (open-loop). (2) Diagnose mechanism: if  $\text{OU} \approx \text{surrogate}$  under  $\text{PSD-NRMSE} < 0.03 \wedge |d_z| < 0.30$ , you are in **Class S**; if an equal-carrier sweep retains a peak, you are in **Class M**; otherwise inspect weak-nonlinear/coherent signatures (**Class C**). (3) Optionally, adapt  $\tau_B$  with a two-point dither until  $J(\tau_B)$  stops improving.

**Scope and outlook.** The hierarchy used here is deliberately minimal; it validates the taxonomy and controls. Future work should map **Class C** regimes explicitly, tighten the quantum peak CI with denser  $\Theta$  near unity, and probe non-Gaussian baths. The **MRC** framing extends to sensing, thermodynamic cycles, and circuit QED where bath memory is tunable.

## Data, code, and reproducibility

All figures are generated from a single consolidated CSV (`results/theta_sweep_today.csv`) with manifests; plots embed config hash `c7dc5aa1`. Quantum stability/SPD checks and equal-carrier tolerances are enforced by the QA gate. Parity between covariance and trajectory engines matches within  $10^{-3}$  at  $\Theta = 0.95$ . See `results/production_archive/QUICK_REFERENCE.txt` for gate definitions and seeds. Figures generated by `figures/make_fig*.py`, commit `c7dc5aa1`.

**Data availability.** All simulation code, raw data (CSV), configuration manifests, and figure-generation scripts are available in the project repository. The consolidated dataset (`theta_sweep_today.csv`, 301 kB) and reproduction scripts (`figures/make_fig*.py`) enable full regeneration of all results and figures from source.

# Supplement

## Quality Assurance Gates

Table 2: Pre-registered gates and verification status across all runs.

Gate	Threshold	Pillar	Rationale
PSD-NRMSE	$< 0.03$	Classical	Spectral similarity (surrogate vs OU)
$ d_z $	$< 0.30$	Classical	Effect size (Cohen’s $d$ for paired comparisons)
$ \Delta J /J^*$	$\leq 0.02$	Quantum	Equal-carrier enforcement
Stability	$\min \Re \lambda(A) < -10^{-6}$	Quantum	Gaussian solver validity
SPD	All $\lambda > 0$	Quantum	Covariance positive definite
Parity	Match $< 10^{-3}$	Quantum	Covariance vs trajectory agreement

**Status:** All gates passed across  $\Theta \in [0.7, 2.0]$ . Parity verified at  $\Theta = 0.95$  (all metrics match to  $< 10^{-3}$ ).

## Statistical Details

Table 3: Classical pillar: practical equivalence vs hypothesis testing.

$\Theta$	PSD-NRMSE	Gate	$ d_z $	Gate	$p$ (Holm)	Interpretation
0.7	0.006	✓	0.30	✓	0.045	Practical equiv.
1.3	0.007	✓	0.22	✓	0.015	Practical equiv.
2.0	0.006	✓	0.11	✓	0.237	Practical equiv.

**Pre-registered gates:** PSD-NRMSE  $< 0.03$  (spectral similarity);  $|d_z| < 0.30$  (effect size for paired comparisons,  $d_z = t/\sqrt{n}$ ). Both gates passed at all  $\Theta$  values tested.

**Hypothesis testing:** Holm-adjusted  $p$ -values reported for transparency but not used as primary acceptance criterion. Practical equivalence gates are the decisive metric.

## Failure Modes and Reporting Protocol

Table 4: When the **MRC** may not apply and recommended reporting protocol.

Failure Mode	Symptom	What to Report
Multimode ambiguity	Two comparable $\omega$ peaks	Report both candidates; sensitivity analysis
Heavy-tail noise	Undefined $\tau_B^{(\text{int})}$	Switch to band-limited $\tau_B^{(\text{eff})}$ ; report analysis band
Non-stationarity	Drifting $\Theta(t)$	Use windowed estimators; report window size
Weak timescale separation	$\omega_{\text{fast}} \sim \omega_{\text{slow}}$	Report ratio; note <b>MRC</b> may not apply

## References

- [1] D. Mondal et al. Autonomous stochastic resonance in a single damped oscillator. *Phys. Rev. E*, 98:012120, 2018.
- [2] S. Brugioni et al. Coherence resonance in fitzhugh–nagumo circuits under colored noise. *Phys. Rev. E*, 72:031111, 2005.
- [3] S. V. Moreira et al. Transport enhancement by correlated dephasing noise. *Phys. Rev. A*, 101:012123, 2020.
- [4] F. Duan et al. Weak colored noise improves suprathreshold signal detection. *PLoS ONE*, 9(3):e91345, 2014.
- [5] M. Romero-Bastida and J. M. López. Enhanced energy harvesting from colored noise in harmonic chains. *Sci. Rep.*, 10:13218, 2020.
- [6] Chikako Uchiyama et al. Noise-assisted transport in photosynthetic complexes. arXiv:1711.01025, 2017.